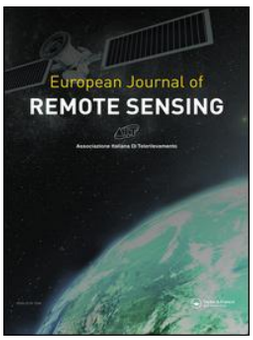

European Journal of Remote Sensing

ISSN: (Print) 2279-7254 (Online) Journal homepage: https://www.tandfonline.com/loi/tejr20

Aerial-based gas tomography – from single beams to complex gas distributions

Patrick P. Neumann, Harald Kohlhoff, Dino Hüllmann, Daniel Krentel, Martin Kluge, Marcin Dzierliński, Achim J. Lilienthal & Matthias Bartholmai

To cite this article: Patrick P. Neumann, Harald Kohlhoff, Dino Hüllmann, Daniel Krentel, Martin Kluge, Marcin Dzierliński, Achim J. Lilienthal & Matthias Bartholmai (2019): Aerial-based gas tomography – from single beams to complex gas distributions, European Journal of Remote Sensing, DOI: 10.1080/22797254.2019.1640078

To link to this article: https://doi.org/10.1080/22797254.2019.1640078

Published online: 13 Jul 2019.

EUROPEAN JOURNAL OF REMOTE SENSING
https://doi.org/10.1080/22797254.2019.1640078

Taylor & Francis
Taylor & Francis Group

Aerial-based gas tomography – from single beams to complex gas distributions

Patrick P. Neumann[a], Harald Kohlhoff[a], Dino Hüllmann[a], Daniel Krentel[a], Martin Kluge[a], Marcin Dzierliński[b], Achim J. Lilienthal[c] and Matthias Bartholmai[a]

[a]Department 8 Non-destructive testing, Bundesanstalt für Materialforschung und -prüfung (BAM), Berlin, Germany; [b]Dział Urządzeń Ciśnieniowych, Urząd Dozoru Technicznego (UDT), Poland; [c]Mobile Robotics & Olfaction Lab, Center of Applied Autonomous Sensor Systems (AASS), School of Science & Technology, AASS Research Centre, Örebro University, Örebro, Sweden

ABSTRACT

In this paper, we present and validate the concept of an autonomous aerial robot to reconstruct tomographic 2D slices of gas plumes in outdoor environments. Our platform, the so-called Unmanned Aerial Vehicle for Remote Gas Sensing (UAV-REGAS), combines a lightweight Tunable Diode Laser Absorption Spectroscopy (TDLAS) gas sensor with a 3-axis aerial stabilization gimbal for aiming at a versatile octocopter. While the TDLAS sensor provides integral gas concentration measurements, it does not measure the distance traveled by the laser diode's beam nor the distribution of gas along the optical path. Thus, we complement the set-up with a laser rangefinder and apply principles of Computed Tomography (CT) to create a model of the spatial gas distribution from a set of integral concentration measurements. To allow for a fundamental ground truth evaluation of the applied gas tomography algorithm, we set up a unique outdoor test environment based on two 3D ultrasonic anemometers and a distributed array of 10 infrared gas transmitters. We present results showing its performance characteristics and 2D plume reconstruction capabilities under realistic conditions. The proposed system can be deployed in scenarios that cannot be addressed by currently available robots and thus constitutes a significant step forward for the field of Mobile Robot Olfaction (MRO).

ARTICLE HISTORY
Received 25 October 2018
Revised 25 June 2019
Accepted 1 July 2019

KEYWORDS
Aerial robot; TDLAS; gas tomography; plume; UAV; mobile robot olfaction; aerial robot olfaction

Introduction

Leaking methane (CH_4) from infrastructures, such as industrial facilities, pipelines and landfills, is critical for the environment and can also pose a safety risk. Therefore, the fast detection and localization of these kind of leaks are of great importance (Bennetts, Schaffernicht, Stoyanov, Lilienthal, & Trincavelli, 2014). Mobile Robot Olfaction (MRO) is the line of research that addresses the task of integrating gas and other environmental sensing modalities (e.g. anemometers) in mobile platforms. MRO started in the early 1990s when the first prototypes were developed and deployed in controlled mock-up environments (Kowadlo & Russell, 2008). Those prototypes were mostly programmed to track gaseous plumes using in-situ gas sensors that need to get in direct contact with gas (such as, e.g. metal oxide sensors) and anemometers for measuring the airflow (Lilienthal, Loutfi, & Duckett, 2006) in an attempt to localize the emitting source. More recently, other tasks like gas distribution mapping, leak localization and gas discrimination have been addressed with ground and aerial robots (Neumann, Asadi, Lilienthal, Bartholmai, & Schiller, 2012; Neumann, Bennetts, Lilienthal, & Bartholmai, 2016; Neumann, Bennetts, Lilienthal, Bartholmai, & Schiller, 2013). Aerial Robot Olfaction (ARO) is a subcategory of MRO that addresses MRO related tasks with aerial robots and deals with the challenges of aerial-based gas measuring. Robots equipped with in-situ gas sensors need to enter the plume in order to detect and eventually identify the gas (Bennetts et al., 2014). This not only limits the applicability of gas sensing mobile robots but also poses a problem for aerial robots that heavily influence the plume propagation by their propulsion system (Neumann, Kohlhoff, Hüllmann, Lilienthal, & Kluge, 2017). Recently, remote gas sensors based on Tunable Diode Absorption Spectroscopy (TDLAS) became commercially available which are suitable to be carried as payload by small Unmanned Aerial Vehicles (UAVs). These sensors can sense a specific gas, e.g. CH_4, up to a distance of 30 m without reflective mirrors or sheets. Remote gas sensors provide integral concentration measurements but no information regarding the distance traveled by the laser diode's beam or the gas distribution over the optical path (Bennetts et al., 2014).

With these new TDLAS sensors, gas tomography became the subject of research for the MRO community (Bennetts et al., 2014; Trincavelli, Bennetts, & Lilienthal, 2012). Gas tomography reconstructs cross-sectional distribution images of the gas plume or cloud

CONTACT Patrick P. Neumann patrick.neumann@bam.de Department 8 Non-destructive testing, Unter den Eichen 87, 12205 Berlin

by incorporating measurements from many different viewing angles (Price, Fischer, Gadgil, & Sextro, 2001). Since the reconstruction quality heavily depends on an accurate estimation of the beam trajectory (Bennetts et al., 2014), it is important to have a system with a stable and reliable localization and orientation.

The key contributions of this paper, which builds upon the work presented in Neumann et al. (2017, 2018), are the validation of a novel aerial robotic platform equipped with a 3-axis gimbal mounted TDLAS sensor, the development of a ray tracer, that is used with the tomographic reconstruction algorithm proposed by Trincavelli et al. (2012), to calculate the endpoint of the laser beam, the setup of a unique outdoor test environment that allows for a quantitative or ground truth evaluation of algorithms in the field of aerial-based gas tomography, and the realization of first outdoor experiments with our robotic platform as a first attempt to estimate the performance of the system in reconstructing 2D slices of a gas plume.

The remainder of this paper is structured as follows: We first give an overview of remote gas sensing and describe related work that addresses detecting CH_4 using TDLAS gas sensors (Sec. 2). In Sec. 3, we present the aerial robotic platform equipped with a 3-axis gimbal mounted TDLAS sensor and elaborate on its development. Next, the experimental scenarios are described (Sec. 5). Finally, we present the experimental results (Sec. 6), draw conclusions and identify directions for future work (Sec. 7).

Related work

Remote gas sensing technologies, such as Tunable Diode Laser Absorption Spectroscopy (TDLAS), emerged in the '90s and constitute an alternative to traditional in-situ gas sensors (Bennetts et al., 2013). Instead of reporting point measurements, TDLAS sensors measure concentrations remotely and report them as integral measurements over the entire path of the beam. TDLAS sensors rely on well-known spectroscopic principles: Gas molecules absorb energy in narrow bands around specific wavelengths in the electromagnetic spectrum (Frish, Wainner, Green, Laderer, & Allen, 2005). Outside these bands, there is basically no absorption (Frish et al., 2005). Thus, the laser diode of a TDLAS sensor can be tuned to the absorption band of the target gas (e.g. CH_4 (Frish et al., 2005)) and modulated in a way that the emitted laser beam is driven on and off the wavelength of interest (Bennetts et al., 2013). During this process, the power of the received laser beam is measured continuously and, by comparing the measurements when the beam is on the target wavelength against the measurements when the beam is off, it is possible to determine with a high degree of selectivity to a specific gas, whether the emitted laser beam has traversed a concentration patch or not (Bennetts et al., 2013). More recently, smaller and lighter TDLAS sensors emerged allowing their usage as payload for mini UAVs (Tokyo Gas Engineering Co. Ltd, 2013). Here, we define a UAV to be classified as mini UAV, when its total takeoff weight ranges from 2 kg to less than 25 kg.

In the following, previous work related to the detection of CH_4 using TDLAS gas sensors is presented: Frish et al. (2005, 2013) and Yang et al. (2018) demonstrated that TDLAS sensors mounted on different vehicles (car, airplane, small UAV) are able to identify areas with CH_4 concentration. However, no further processing of the measured integral concentrations and/or no further 3-axis stabilization with the possibility to orient the sensor were proposed. Ro, Johnson, Varma, Hashmonay, and Hunt (2009) estimated CH_4 concentrations from agricultural sites using a pan-tilt mounted TDLAS sensor and an array of retroreflectors. The estimation of the total amount of emitted CH_4 per time unit was the focus of the project. Grinham, Dunbabin, Gale, and Udy (2011) attached a single-path Optical Methane Detector (OMD) to an Autonomous Surface Vessel (ASV, robotic vessel) in order to map areas of ebullitive CH_4 emissions and to estimate the spatial-temporal release rates across an entire water storage site. Soldan et al. proposed a mobile robot called RoboGas$^{\text{Inspector}}$ for routine inspections in large industrial environments (Soldan, Bonow, & Kroll, 2012). The mobile robot is equipped with a pan-tilt mounted sensor head consisting of, i.a., a TDLAS sensor and a thermographic camera for gas visualization. In (Bonow & Kroll, 2013), the authors presented a gas source localization strategy based on triangulation for this system. Bennetts et al. (2013) introduced a robotic platform called Gasbot that aims to automatize methane emission monitoring on landfills and biogas production sites using a pan-tilt mounted TDLAS sensor unit. In addition, the authors proposed a method to create 3D CH_4 concentration maps from integral concentration and depth measurements (Bennetts et al., 2014). Recently, Tannant et al. (2018) and Emran, Tannant, and Najjaran (2017) presented results of a UAV-mounted TDLAS sensor for detecting fugitive greenhouse gases leaks. However, so far, no aerial-based system equipped with a 3-axis gimbal mounted TDLAS sensor was developed and proposed for MRO tasks.

Computed Tomography for Gases (CTG) is the task of deriving gas distribution models from localized integral concentration measurements (Bennetts et al., 2014; Byer, 1979; Price et al., 2001). CTG models can be either grid-based or parametric: grid-based approaches estimate the concentrations at each cell from a set of integral concentration measurements (Haruta & Ogawa, 2005; Trincavelli et al.,

2012), whereas parametric approaches use, e.g. the integral measurements to fit functional parameters of an analytic function, e.g. a set of n basis functions (Drescher, Gadgil, Price, & Nazaroff, 1996). In this work, we use a grid-based approach first presented in (Trincavelli et al., 2012).

A common approach in CTG is to use fixed sensing configurations, i.e. the emitting laser diodes/reflectors are placed at predefined positions (Bennetts et al., 2014). This has the advantage that the optical paths of the beams are well known. However, robots equipped with remote gas sensors need to estimate the optical path, which heavily depends on its localization and orientation accuracy. Furthermore, it is also important to select optimal measuring poses, as the reconstruction quality depends heavily on the chosen sensing geometry (Arain, Schaffernicht, Hernandez Bennetts, & Lilienthal, 2016; Arain, Trincavelli, Cirillo, Schaffernicht, & Lilienthal, 2015). The work presented in (Trincavelli et al., 2012) and (Bennetts et al., 2013) is the first attempt towards Robot-Assisted Gas Tomography (RAGT) with a ground-based robot, whereas this work constitutes the first attempt towards RAGT with an aerial robot.

The UAV-REGAS platform

The German Federal Institute for Materials Research and Testing (BAM) has developed a new aerial-based measuring system as part of an interdisciplinary in-house R&D project named "Complex Fires – Consequences of accidental failure of gas tanks" (CoFi-ABV).[1] The R&D project focuses on the examination of the consequences and the impact of failure of gas tanks for alternative fuels for vehicles considering complex fire and explosion scenarios. The project comprises a multitude of destructive tests in real scale.

One aim of the project is the integration of a robust open-path gas detector into a mini UAV for remote sensing of gas clouds, tomographic reconstruction of gas plumes and precise localization of gas sources. Our goal is to provide for rescue units such as firefighters a powerful and robust tool for helping to assess the specific dangers related to gas leaks, their extension and the dimension of the danger zone.

Robotic platform

The DJI Spreading Wings S1000+ octocopter (in the following referred to as mini UAV, see Figure 1) has a diagonal wheelbase of 1045 mm. The mini UAV weighs 4.4 kg and has a maximum takeoff weight of 11 kg. Its maximum flight time depends, i.a., on the takeoff weight and prevailing wind conditions. According to the manufacturer's data sheet (DJI, 2016), the mini UAV can achieve flight times of up to 15 min using a 6S 15,000 mAh battery pack (tested on a windless day with 9.5 kg takeoff weight, hovering at a height of 2 m). As flight controller, we use the DJI A3 Pro multi-rotor stabilization controller. Besides a ROS interface for autonomous waypoint navigation, flight data access, gimbal and aircraft control through its onboard SDK, the new controller is equipped with three Inertial Measurement Units (IMU) and three Global Navigation Satellite System (GNSS) units for better flight stability and redundancy. A 2.4 GHz full HD digital video link is

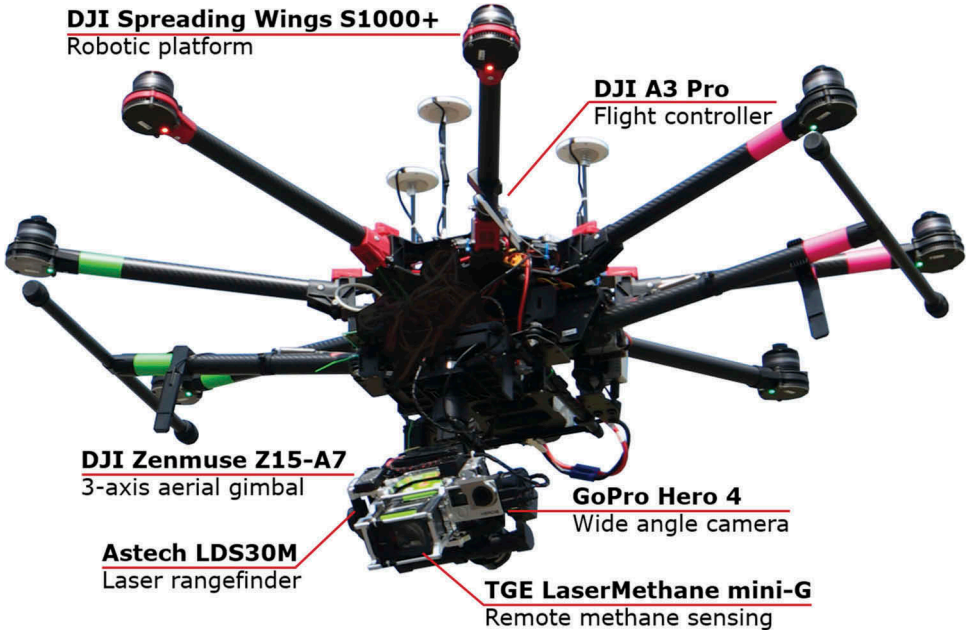

Figure 1. UAV-REGAS platform: DJI Spreading Wings S1000+ octocopter equipped with the 3-axis aerial stabilization gimbal mounted TDLAS sensor as payload. The sensors used in this paper are explained in the text.

[1]BAM focus area "infrastructure".

established by the DJI Lightbridge that also allows to remotely control the mini UAV.

To improve altitude estimation, we installed a SF20 laser rangefinder (LightWare Optoelectronics Ltd., South Africa) on the mini UAV pointing downwards. This laser module weighs only 10 g and has a measurement range up to 100 m using a class 1M laser. The SF20 has a resolution of 10 mm with a measuring accuracy of ±100 mm and offers sampling rates from 48 Hz to 388 Hz.

As onboard computing unit, we use the UDOO X86 as it provides sufficient computing power, GPIOS and communication interfaces such as UART or I^2C. We installed a Dual Band MIMO Wi-Fi module (802.11ac), which is used as a wireless radio link. Both, the UAV's flight controller and the UDOO computing unit, are connected via UART.

Mobile ground station

For controlling our UAVs and their payloads, we built up a mobile ground station running a customized version of the APM Planner 2 from ArduPilot for path planning. The ground station consists of 100 Ah battery, a 12 V pure sine wave power inverter with 650 W (FraRon electronic GmbH), a battery charger type Atlas-300IM (MEC-Energietechnik GmbH) and a docking station that is connected to two monitors and a D-Link DAP-2695 WLAN access point. This setup allows us to keep the ground control station operational at least for 4 h without an external electrical power supply.

Sensor integration

In this work, we use the Laser Methane mini-G (SA3C50A, in the following, referred to as LMm-G) manufactured by Anritsu and distributed by Tokyo Gas Engineering to measure CH_4 concentrations. The LMm-G belongs to the family of TDLAS gas sensors. In comparison to traditional gas sensing modalities, these sensors do not require a direct interaction between the sensor's surface and the target compound (Bennetts et al., 2013). Instead, the LMm-G measures concentrations remotely and reports them as integral measurements in ppm·m. However, the LMm-G does not provide any information regarding the distance traveled by its beam. The measuring principle of the LMm-G is shown in Figure 2. The LMm-G has a dimension of 70 × 179 × 42 mm^3 and weighs approximately 530 g including the battery. According to the manufacturer's data sheet (Tokyo Gas Engineering Co. Ltd, 2013), it is able to measure CH_4 concentrations in the range from 1 ppm·m to 50,000 ppm·m. It offers a fast response (0.1 s) and high sensitivity. The detection distance ranges from 0.5 m to 30 m. The beam has a cone shape with an opening angle of θ_{LMm-G} = 8.5 mrad ≈ 0.5° or less, which means that always a volume is measured (the projected area of the beam has a diameter of 0.17 m at 20 m). A built-in standard gas cell allows an auto-calibration and self-check during startup of the device that will be automatically repeated in case of wavelength stability errors. To interface with the LMm-G, the built-in bluetooth module was replaced with a custom-built circuit board that enables a serial communication via UART.

Figure 3 shows the payload comprising a modified 3-axis aerial gimbal (DJI Zenmuse Z15-A7) for stabilizing and orienting the sensors, the open-path gas detector LMm-G, a laser module for distance measurements (Astech LDS30M) and a wide-angle camera (GoPro Hero 4), that allows creating CH_4 scans and documentation of the exploration area (Neumann et al., 2017). The payload is balanced in the center of the three gimbal axes. The gimbal allows rotation angles of ±360° (yaw), +50°/−140° (pitch) and ±40° (roll) with a control precision of ±0.01°. This allows to counteract even small compensation movements by the UAV caused by wind gusts, for example. In addition, by rotating the sensor a large area can be scanned without the need to pilot a new waypoint. An additional 10 DoF IMU board, that consists of a 3-axis accelerometer, a 3-axis gyroscope, a 3-axis magnetometer and a barometric pressure sensor, is used to generate control signals for the gimbal. Currently, a Mahony filter

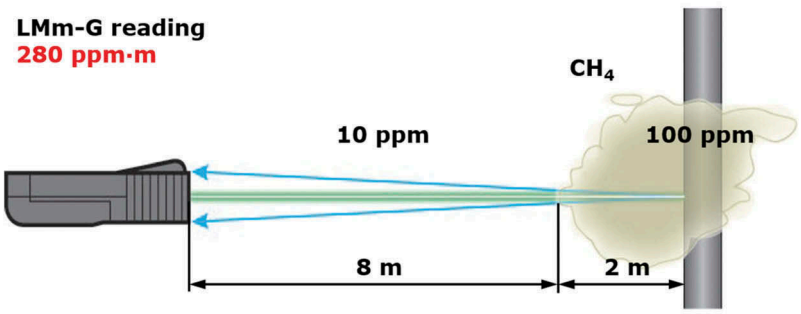

Figure 2. Measurement principle of the LMm-G. Here, the device reports an integral concentration measurement of 280 ppm·m with the infrared beams traveling a 10 m path, in which a background concentration level of 10 ppm and a methane patch of 200 ppm are present (10 ppm × 8 m + 100 ppm × 2 m = 280 ppm·m).

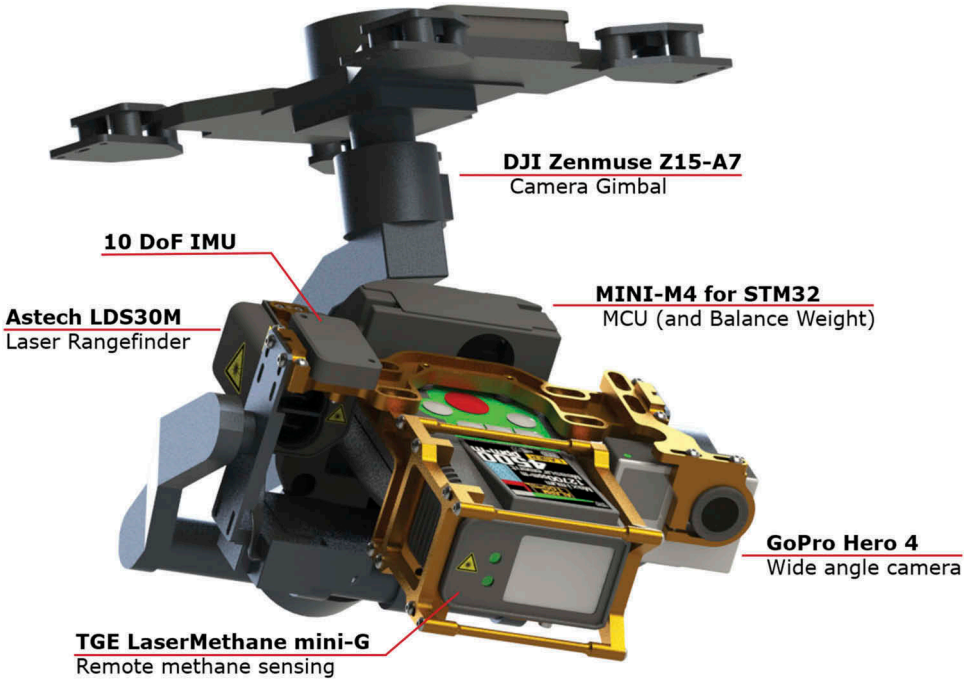

Figure 3. Detailed view of the open-path gas detector installed on the 3-axis aerial stabilization gimbal.

estimates the gimbal's attitude during operation and supervises its exact positioning (Mahony, Hamel, & Pflimlin, 2008). While being positioned, the rotating gimbal induces a torque that has to be compensated by the flight controller. There was no impact on the flight stability observable while the gimbal performed the rather small compensating motions during the measurements. This might be different, however, if smaller carrier platforms were used. The laser module LDS30M weighs 50 g and has a measurement range from 0.2 m to 30 m for target reflectances of ≥10%. The LDS30M has a resolution of 10 mm with a measuring accuracy of ±50 mm and offers sampling rates of up to 30 kHz. The purpose of the laser distance measurement system mounted next to the LMm-G is to collect range information. A small microcontroller board (small ARM Cortex-M4 development board called MINI-M4, MikroElektronika) located on the gimbal collects all relevant data from these sensors and transfers it to the UDOO X86 platform, which logs the received data, transfers it over Wi-Fi to the ground station and moreover controls the gimbal's attitude by creating Futaba S.Bus input signals. The payload can perform automatic scans of the area of interest or may be controlled manually from the ground station using an Xbox controller.

Plume reconstruction algorithm

The TDLAS sensor measures CH_4 concentrations remotely and reports them as integral measurements in ppm·m over the distance traveled by the beam. This scenario is similar to computed tomography (CT), where the image of a body is reconstructed from a set of attenuation measurements of, e.g. X-ray beams (Bennetts et al., 2014). In contrast to CT which images fixed structures like bones, gas tomography has to deal with highly dynamic effects since gas disperses in the environment due to airflow advection and turbulence (Bennetts et al., 2014). In the following, we will describe how to estimate a model of the gas distribution, more precisely how to reconstruct 2D slices of a gas plume, that captures its statistical properties. A 3D reconstruction of the plume can then be obtained by arranging multiple 2D slices one against the other.

Ray tracing

The beam's starting point $p_1 = (\lambda_1, \varphi_1, h_1)$ is determined using the mini UAV's onboard GPS only, where λ is the longitude, φ is the latitude and h is the altitude of the coordinate (Figure 4). Then, the beam's endpoint $p_2 = (\lambda_2, \varphi_2, h_2)$ is estimated using attitude and heading information of the gas sensor.

First, the distance between both points projected on flat ground $d(p_1, p_2)$ is estimated with

$$d(p_1, p_2) = d_{\text{TDLAS}} \sin(\theta_{\text{pitch}}), \tag{1}$$

where d_{TDLAS} is the distance traveled by the laser diode's beam measured by the payload's laser rangefinder and θ_{pitch} is the estimated pitch angle of the payload. Then, the difference in altitude between both points Δh is calculated based on Eq. 2.

$$\Delta h = h_1 - \sqrt{d_{\text{TDLAS}}^2 - d(p_1, p_2)^2}, \tag{2}$$

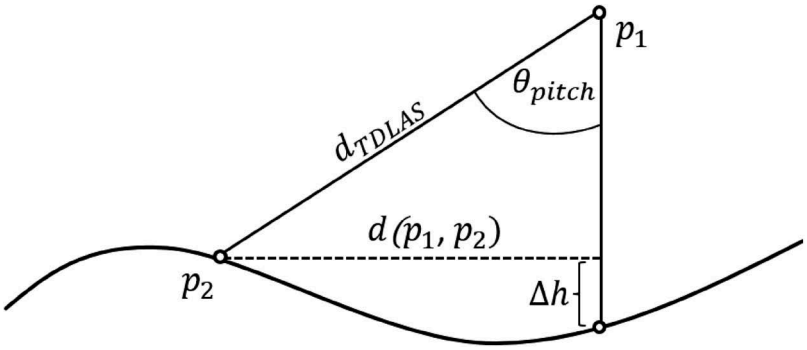

Figure 4. Ray tracing of the laser beam of the TDLAS sensor.

where h_1 is the altitude of the payload measured by the mini UAV's laser rangefinder. The calculation of h_2 can be derived from Eq. 2.

Finally, longitude and latitude of the beam's endpoint are calculated using longitude and latitude of the beam's starting point, the compass heading of the payload α, and the distance $d(p_1, p_2)$ determined in Eq. 1 based on great circle approximation.

$$\varphi_2 = \sin^{-1}\left(\sin\left(\varphi_1\right)\cos(r) + \cos\left(\varphi_1\right)\sin(r)\cos(\alpha)\right) \tag{3}$$

$$\lambda_2 = (\lambda_1 + d_{\lambda_2} + \pi) \bmod (2\pi) - \pi \tag{4}$$

with

$$d_{\lambda_2} = \operatorname{atan2}\left(\sin(\alpha)\sin(\mathrm{r})\cos(\varphi_1), \cos(\mathrm{r}) - \sin(\varphi_1)\sin(\varphi_2)\right) \tag{5a}$$

$$r = \frac{d(p_1, p_2)}{6378137\ \mathrm{m}} \tag{5b}$$

Note that the payload automatically compensates disturbances on both the roll and yaw axis. Thus, for simplification purposes, we consider these angles to be constant over time.

Gas distribution mapping

For reconstructing 2D slices of the plume, we use a tomographic reconstruction algorithm first proposed by Trincavelli et al. (2012), where the problem of gas distribution modeling is treated as an optimization problem. Like traditional CT algorithms, this algorithm updates a grid model using the integral measurements from the TDLAS sensor.

The algorithm decomposes the integral concentration measurements y reported by the TDLAS sensor as follows:

$$y = \sum_{i=1}^{M} l_i x_i + \varepsilon, \tag{6}$$

where M is the number of grid cells traversed by the TDLAS beam, l_i is the distance traveled by the beam in cell i, x_i is the concentration in grid cell i and ε is the measurement noise term. Figure 5 shows an example of the decomposition of the integral concentration measurements.

The gas distribution mapping task is then formulated as the problem of estimating the concentration vector $\vec{x}$ which best explains a set of N measurements. Accordingly, the measurement dataset becomes an $N \times M$ matrix described by the following equation:

$$\vec{y} = \vec{L}\vec{x} + \varepsilon\vec{1}, \tag{7}$$

where $\vec{L}$ is a $N \times M$ matrix that contains the traversed distances for each measurement, $\vec{x}$ is a column vector of length M that contains the concentration values for the traversed grid cells and $\vec{1}$ is a column vector of ones of length N. A Gaussian distribution is assumed for ε, which means that the noise in the TDLAS sensor is unbiased. In addition, a Gaussian prior distribution over $\vec{x}$ is defined to limit the number of solutions. Thus, this problem can be formulated as the following optimization problem:

$$\begin{aligned} &\underset{\vec{x}}{\text{minimize}} && \| \vec{L}\vec{x} - \vec{y}\|_2 + \lambda \| \vec{x}_2\|_2 \\ &\textit{subject to } \vec{x} \geq 0 \end{aligned} \tag{8}$$

where λ is a parameter determining the strength of the prior and the constraint $\vec{x} \geq 0$ is added to discard negative gas concentration measurements (which would not make sense).

Experimental scenarios

All experiments were performed outdoors on the BAM Test Site for Technical Safety (BAM TTS). The experimental area is surrounded by trees and buildings, which introduced a certain level of turbulence.

System characterization

For the first scenario, we investigated for a maximum allowed payload deflection angle, the reflectivity properties of different surfaces typical for landfills (bright sand, dark sand and vegetation) at different measuring

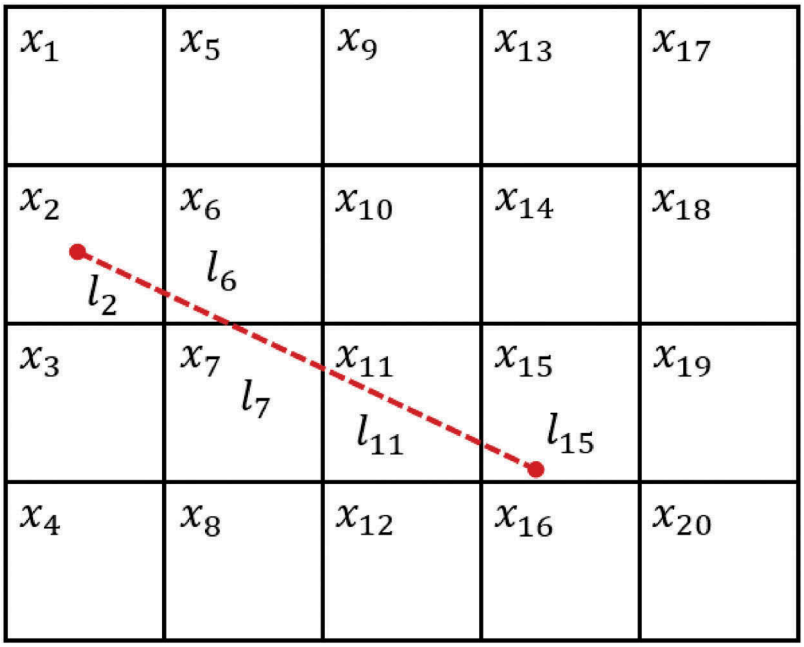

Figure 5. Exemplary decomposition of a TDLAS beam (denoted by a red dashed line) traveling inside a 4 × 5 grid. The integral measurement is decomposed as $y = l_2 \cdot x_2 + l_6 \cdot x_6 + l_{11} \cdot x_{11} + l_{15} \cdot x_{15} + \varepsilon$, where ? is the measurement noise. Figure and caption are reproduced from Trincavelli et al. (2012).

distances (10, 15 and 20 m). For this purpose, gas measurements with the mini UAV on the ground were performed against an earth wall that has a slope angle of approximately 30° (see Figure 6a). The measurements were recorded at a sampling frequency of 2 Hz and for each trial, data were collected over a period of 40 s. As a gas source, we used a small, sealed glass cube (edge length of 0.2 m) filled with 2.5%$_{vol}$ CH_4 that was placed in front of the TDLAS sensor in an angle of 45° to avoid interreflection inside the cube (see Figure 6a, highlighted in red). This means that we expect the TDLAS sensor to measure concentrations of around 5,000 ppm·m (2.5%$_{vol}$ × 0.2 m) assuming a negligible background concentration. Each time the glass cube was repositioned in front of the TDLAS sensor, reference measurements against a white reflecting sheet in a distance of ≤0.5 m were performed. The repositioning of the glass cube may have affected marginally the length of the laser beam traveling inside the cube and therewith as wellthe actual measurements. As in Bennetts et al. (2013), this setup does not capture the complexities of gas dispersal escaping from an actual leak, since the CH_4 is kept isolated from the testing environment inside a glass cube. However, for this initial evaluation repeatable conditions were required, and it can be assumed that the concentration levels remain fairly the same during the different trials.

In the second scenario, the performance of the mini UAV system in automatic scanning mode while hovering was investigated. For this, the mini UAV was deployed in GPS attitude mode, where it

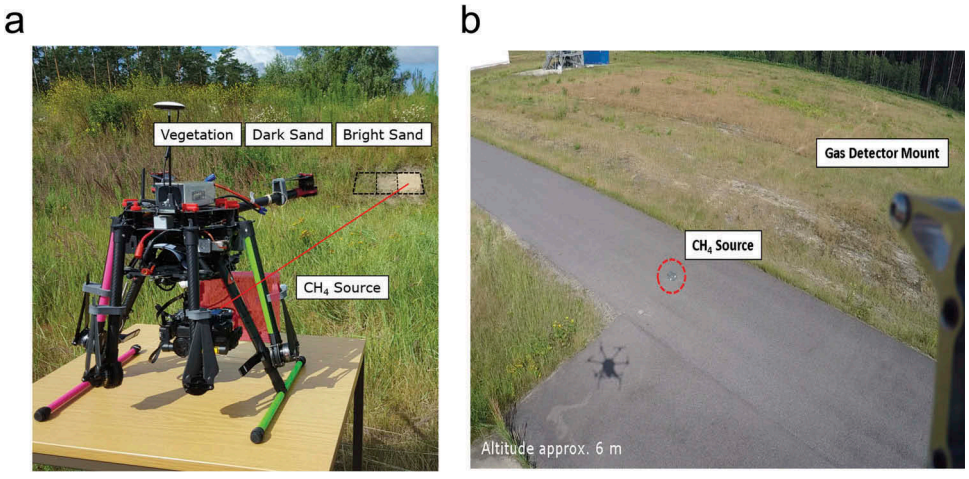

Figure 6. Experimental scenarios: (a) on ground and (b) in flight.

tries to keep the attitude stable and to lock the aircraft position accurately. The experiment started after the mini UAV reached the target position at an altitude of approximately 16 m. Data were collected during the time span of the experiment (200 s).

For the third scenario, we simulated a leakage (for example, from a broken pipeline underneath an asphalt street) at a known position. As a gas source, we used the above-described CH_4 filled glass cube (Figure 6b). The mini UAV and its payload were remotely operated to perform gas measurements at different altitudes (approximately 5, 10, 15 and 22 m) while trying to aim at the glass cube using the real-time video link. Note that, in all experimental setups, no artificial reflective surfaces were installed – ground reflection alone was sufficient for the TDLAS sensor.

Plume reconstruction

The plume reconstruction experiments were conducted on two different days, where an artificial gas source was placed within the experimental area (see Figure 7). The gas source was a gas cylinder bundle of natural gas (approx. 90% CH_4) connected to small tubes, which were attached to a fan in order to spread the analyte away from the outlet. The air current introduced by the fan also prevented the CH_4 to immediately rise up to the atmosphere when released. The artificial gas source had a more or less constant release rate over the duration of the experiment as the pressure-reducing valve was set to a constant pressure of approximately 15 bar.

Two ultrasonic anemometers (uSonic-3 Scientific (former: USA-1), Metek GmbH, Germany) were mounted at a height of 2 m (in the following referred to USA1) and 4 m (USA2), respectively, at a distance of approximately 3 m from each other as shown in Figure 7. The ultrasonic anemometers have an operating range of 0 up to 60 m/s with a resolution of 0.01 m/s and an accuracy of ±0.1 m/s. The resolution of the wind direction is 0.1° with an accuracy of ±2°. The wind measurements were recorded at a frequency of 1 Hz during the experiments.

The experiments were supported by a distributed array of 10 pressure-capsulated, highly dynamical infrared gas transmitters (PIR7000, Dräger Safety AG & Co. KGaA, Germany) with a response time of t_{90} = 1 s to allow for a quantitative or ground truth evaluation (Neumann et al., 2017). This very short response time also allows resolving the temporal dimension of gas distribution processes. These gas sensors were mounted on an aluminum metal frame cube with a dimension of 2 × 2 × 2 m^3, which can be seen in Figure 7. The gas measurements were recorded also at a frequency of 1 Hz during the experiments.

In each experiment, the mini UAV was programmed to explore the experimental area following a simple trajectory consisting of 5 waypoints (Figure 7), starting from a remote location and moving at 1 m/s between the measuring positions. The waypoints were obtained by consecutively placing the mini UAV on the markings that are highlighted in Figure 7. During the exploration, the robot was stopping at the waypoints to collect gas measurements. At each measuring position, the gimbal was used to scan the area with a discontinuous sweeping movement with an aperture of (−60°; −120°) in pitch (the payload is oriented downwards, when θ = −90°) with a step size of 5°. Take-off and landing were performed manually. Each trial took 3 to 4 min to complete. During two days, a total of 26 trials could be performed.

Note that, again no artificial reflective surfaces were installed – ground reflection alone was sufficient

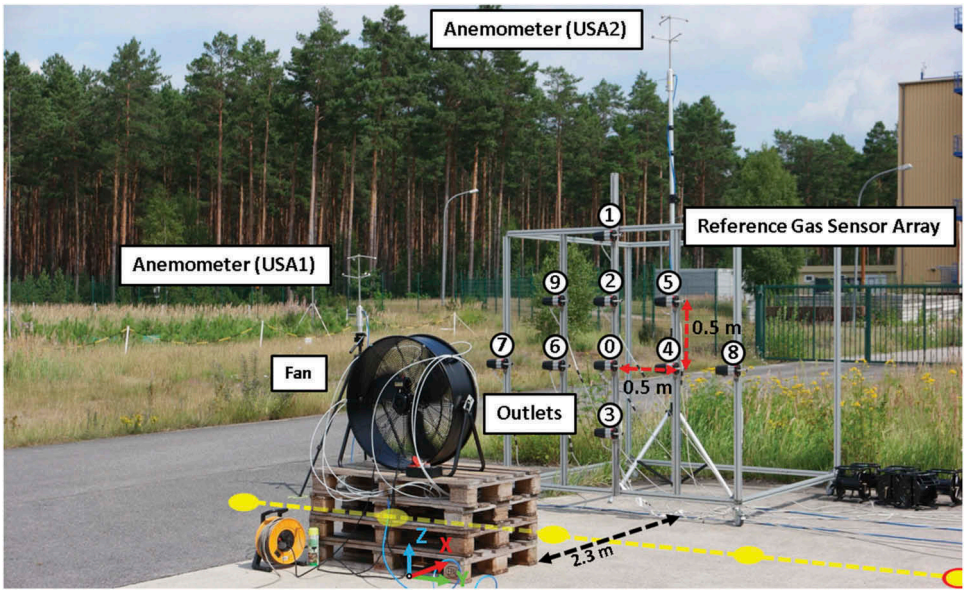

Figure 7. Experimental setup of the plume reconstruction experiments.

for the TDLAS sensor. Furthermore, the trajectory was planned in a way that the experimental installation did not have a significant effect on the integral gas measurements performed by the mini UAV.

Experimental results

System characterization

Figure 8 and Table 1 show the results of experiment #1 (earth wall barrier experiments). The values in Table 1 are given as confidence intervals with 95% confidence level for the mean (assuming normally distributed data), where non-valid data (see Table 1 for more details) were excluded from the calculation. Trial #1 refers to a measurement of the CH_4 background concentration, trial #2 is the actual measurement of the CH_4 and trial #3 is the reference measurement against a white reflecting sheet. The measurements are reproducible, and the mean concentrations lie mostly within the claimed measurement accuracy of ±10% of the TDLAS sensor (Tokyo Gas Engineering Co. Ltd, 2013). An exception constitutes trial #2 performed on dark sand at 20 m that has a significantly higher variance in the measurements and an average accuracy of approximately 13%, and trial #2 performed on vegetation at 20 m, where only 45.3% of the measurements were valid (the remaining measurements were marked with the error code for not enough reflection by the TDLAS sensor). Based on these observations it can be assumed that the TDLAS sensor requires at least 2% intensity of the reflected laser beam to work properly. Of course, the level of reflectivity depends essentially on the (reflecting) surface. Furthermore, the results indicate that the variance in the gas measurements increases as the measuring distance increases, corresponding to the expected decrease in the intensity of the received laser beam decreases (compare Figure 8 and Table 1). With increasing distance, also the integrated CH_4 background concentration increases as expected (trial #1). However, an exception constitutes the measurements performed in trial #3 on bright sand at 15 m, which are much lower than at 10 m. From these results, we arrived at the following ranking regarding the reflecting properties (from good to poor): (1) bright sand, (2) dark sand and (3) vegetation.

The results of experiment #2 (automatic scanning mode experiments) can be seen in Figure 9b. Comparing the different trials with each other gives an RMSE of 1.19° (target angle vs. on ground), 1.92° (target angle vs. airborne) and 1.49° (on ground vs. on airborne) for the payload's pitch angle θ. The mean pitch angle θ over all available IMU data corrected with the target angle is −0.26° with a standard deviation of ±1.86°. The error in compensating the roll angle φ can be neglected as the TDLAS sensor is mostly aligned within the center of this axis. As the yaw axis is fixed during scanning mode, the angle ψ can be neglected as well. The accuracy of the distance

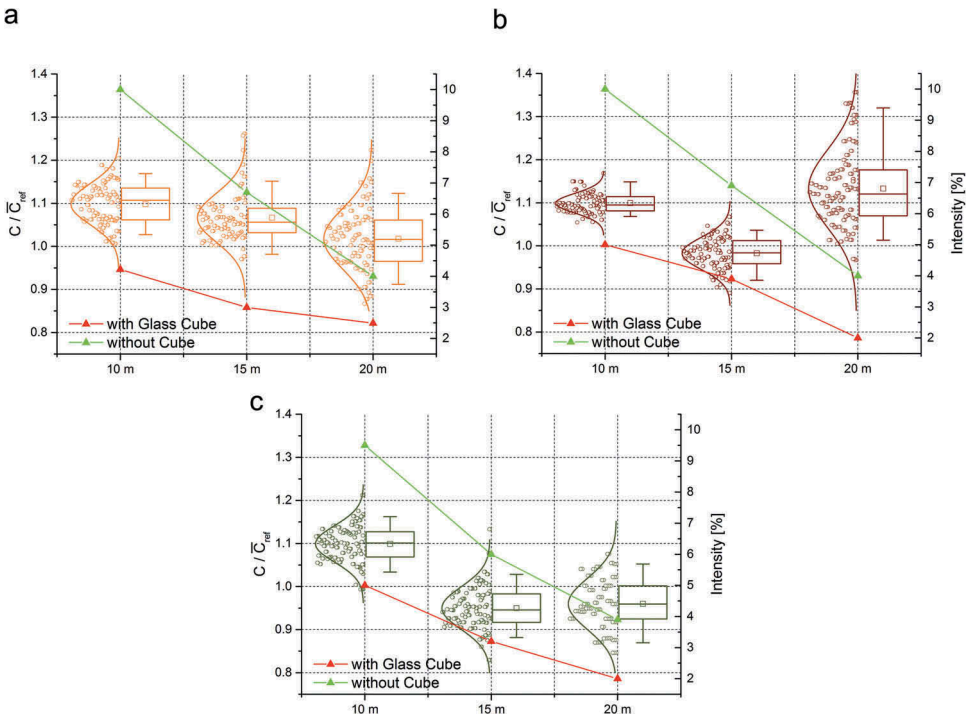

Figure 8. Results of the earth wall experiments for (a) bright sand, (b) dark sand and (c) vegetation. The box-plots show the measured concentrations normalized by the averaged reference measurement. The box shows the lower/upper quartile and the line denotes the median. The mean is denoted by a small squared marker and the whiskers represent the 5% and 95% quantiles. Next to each box also the data points and the corresponding distribution curves (assuming normally distributed data) are shown. The red and green curves show the decrease in intensity of the received laser light while increasing the measuring distance with and without glass cube, respectively.

Table 1. Results of the earth wall experiments.

Surface	Trial #	Measuring distance (m)	CH_4 Concentration (ppm·m)	Intensity (%)
Bright Sand	1	10.40 ± 0.004	55.2 ± 3.1	10.0 ± 0.0
	2	10.57 ± 0.004	4241.5 ± 25.2	4.2 ± 0.1
	3	0.41 ± 0.003	3862.6 ± 13.0	67.4 ± 0.5
	1	14.39 ± 0.004	28.1 ± 2.6	6.7 ± 0.1
	2	14.40 ± 0.004	4119.3 ± 30.3	3.0 ± 0.0
	3	0.44 ± 0.003	3669.9 ± 14.0	15.3 ± 0.1
	1	20.42 ± 0.006	66.8 ± 6.4	4.0 ± 0.0
	2	20.49 ± 0.012[1]	3930.5 ± 37.6	2.5 ± 0.1
	3	0.43 ± 0.006	3703.5 ± 8.2	18.2 ± 0.6
Dark Sand	1	10.37 ± 0.003	29.5 ± 2.3	10.0 ± 0.0
	2	10.38 ± 0.003	4148.2 ± 11.9	5.0 ± 0.0
	3	0.41 ± 0.003	3774.0 ± 6.9	96.9 ± 0.6
	1	14.36 ± 0.005	49.1 ± 2.6	6.9 ± 0.1
	2	14.31 ± 0.140	3707.7 ± 19.4	3.9 ± 0.0
	3	0.45 ± 0.004	3377.0 ± 12.1	24.7 ± 1.6
	1	20.48 ± 0.006	58.7 ± 5.1	4.0 ± 0.0
	2	20.51 ± 0.256[1]	4275.3 ± 47.0	2.0 ± 0.0
	3	0.44 ± 0.040[1]	3795.1 ± 17.4	12.7 ± 0.1
Vegetation	1	10.30 ± 0.005	29.2 ± 2.6	9.5 ± 0.1
	2	10.31 ± 0.005	4194.0 ± 22.2	5.0 ± 0.0
	3	0.42 ± 0.003	3815.6 ± 14.8	13.4 ± 0.1
	1	14.19 ± 0.005	46.1 ± 4.2	6.0 ± 0.0
	2	14.22 ± 0.006	3624.8 ± 25.7	3.2 ± 0.1
	3	0.46 ± 0.007	3277.0 ± 9.6	37.3 ± 2.3
	1	20.33 ± 0.199	70.9 ± 7.0[2]	3.9 ± 0.0
	2	20.51 ± 0.027	3661.8 ± 46.3[3]	2.0 ± 0.0
	3	0.44 ± 0.005	3994.5 ± 8.0	15.1 ± 0.2

[1]5%, 20% and 1% (in the order of appearance) of the distance measurements were not valid (LDS30M sensor reported the error code for no aim).
[2]As high as 18.9% of the gas measurements were not valid (TDLAS sensor reported an unknown error code).
[3]As high as 54.7% of the gas measurements were not valid (TDLAS sensor reported the error code for not enough reflection).

measured with the laser module can be extracted from Table 1. The mean deviation over all available barometric altitude data to the commanded altitude of the mini UAV is 0.10 m with a standard deviation of ±0.08 m, for the orientation, the deviation is 0.27°± 0.27. The mean distance over all available GPS data to the commanded waypoint of the mini UAV is 0.25 m with a standard deviation of ±0.12 m. These results indicate that the mini UAV system can hold its attitude and aim the laser beam at a target fairly accurate regardless of changing wind conditions.

Figure 9c shows the results of experiment #3 (leakage experiments). The mini UAV is able to detect the CH_4 filled glass cube on asphalt street in distances of ≤25 m once aiming is completed. As the mini UAV and its payload were controlled remotely by two different operators, it was not possible to realize continuous gas detection. Nevertheless, approximately 30.2% of the time between 25 s and 351 s we were able to detect concentrations above a threshold of 200 ppm·m, which is much higher than the measured CH_4 background concentrations at similar distances (see Table 1).

These results indicate the potential of the UAV-REGAS platform to accurately perform remote gas measurements while aiming at potential gas leaks.

Plume reconstruction

The experiments were performed on two different days under different weather conditions. The first day was cloudy with an average temperature of approximately 25°C. The wind conditions during the first day were relatively stable. The average wind speed was in the range of approximately 1.5 m/s (USA1) to 1.7 m/s (USA2) and the average wind direction was between 216° (USA1) and 212° (USA2) (the wind generated from the fan came approximately from 257° direction). The degree of stability is given by the circular variance S_0 which is a dimensionless number (Gaile & Burt, 1980). Its value varies from 0 to 1, where a lower value indicates more stable wind conditions, whereas a higher value refers to more turbulent conditions. On day #1, S_0 was around 0.32 (USA1) and 0.28 (USA2).

The second day was sunny with an average temperature of 21° C. The average wind speed was in the range of approximately 1.2 m/s (USA1) to 1.3 m/s (USA2) and the average wind direction was between 172° (USA1) and 168° (USA2). The circular variance was around 0.47 (USA1) and 0.41 (USA2) indicating a stronger variance than on the first day and thus representing rather unstable wind conditions.

Figure 10 shows three example reconstructions of the 2D gas distribution using the corresponding available measurement data of each trial. It can be noticed that, in all mean maps, high concentrations (denoted by darker shades) are predicted at locations near the centerline of the plume at heights between 1 and 2 m. Most of the neighboring cells of these high concentration regions show no or only very small concentrations that could be a result of the turbulent nature of gas dispersal or the fact that these cells were

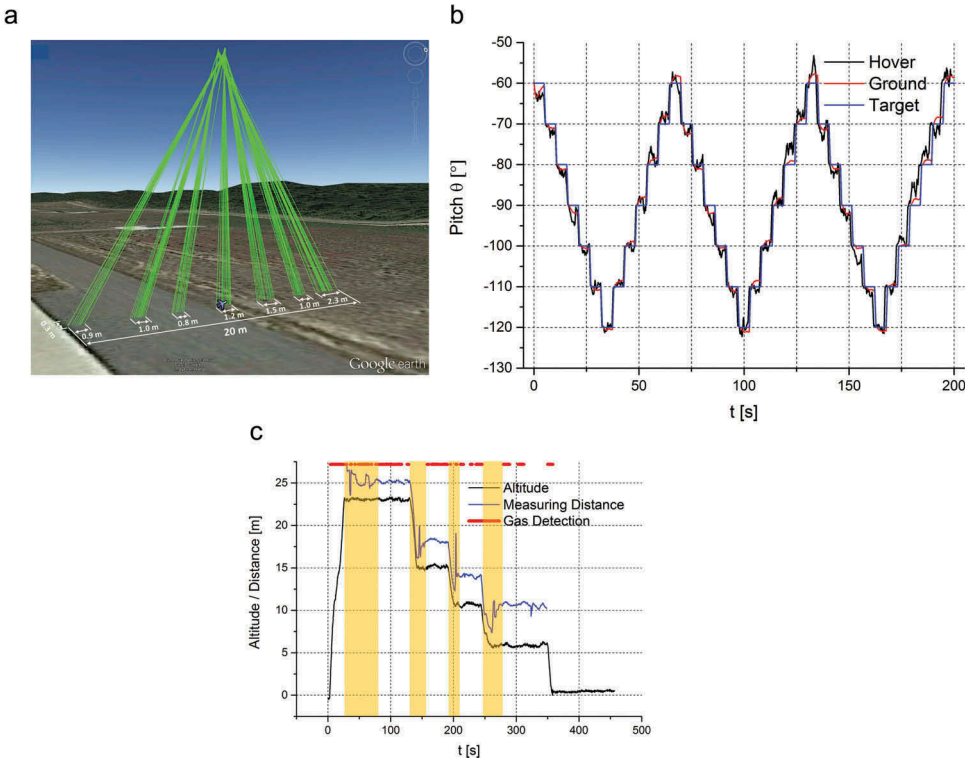

Figure 9. (a) Visualization of the TDLAS beams of one sweep while the mini UAV hovered in an altitude of approximately 16 m. (b) Comparison of the scanning mode trials: the blue, red and black curves represent the target pitch angle, the pitch angle while the mini UAV was on the ground and the pitch angle while the mini UAV was airborne, respectively. (c) Results of the leakage experiments: the black and blue curves show the altitude of the mini UAV and the measuring distance obtained from the laser module, respectively. The orange areas denote approximately the time needed for aiming the payload at the glass cube. The glass cube is defined to be detected if the measured concentration is >200 ppm·m (red line).

not traversed by the beams. Furthermore, concentrations below approximately 1500 ppm are predicted in the boundary area of the laser beams which could be a result of insufficient sensor data. Additionally, in all variance maps, the beams of the TDLAS sensor are indirectly visible, and the high variance contributions at the beams starting locations are probably a result of the highly fluctuating integral gas concentration measurements performed at a single waypoint with different gimbal pitch angles.

The interaction between the released CH_4 and the environment creates complex structures, where turbulence can meander the plume while airflows can move the CH_4 patches away from the source (Bennetts, Lilienthal, Khaliq, Pomareda Sesé, & Trincavelli, 2012). This probably is also reflected in the generated map of Figure 10b, where high concentration cells are spread over the measured area.

Figure 11 presents exemplary the response of the reference gas sensor array during trial #4 performed on day #1, whereas Figure 12 shows the corresponding calculated end points of the laser beams, the trajectory of the mini UAV and the piloted waypoints. During that trial, the mean concentration varied between 48 ppm ± 213 ppm (sensor 1) and 1474 ppm ± 2069 ppm (sensor 3). During that trial, sensor 3 measured the highest concentration of 8811 ppm. The results of the remaining trials show similar means and peak concentrations. Furthermore, it can be noticed that the measured and reconstructed gas concentrations are within the same magnitude.

Although these first results indicate the potential of the UAV-REGAS platform to perform 2D plume reconstruction, Figure 12b demonstrates clearly that the accuracy of GPS is not sufficient for applications, where accurate gas source localization and gas distribution mapping are required.

Conclusion and future work

In this work, we present a prototype of an aerial robotic platform called UAV-REGAS aimed at gas source localization and gas distribution mapping tasks by using its remote sensing capabilities. In contrast to a UAV equipped with traditional in-situ chemical sensors (such as metal oxide sensors), our proposed approach offers:

- highly selective measurements of the target gas,
- remote gas measurements, i.e. no direct contact with the gas plume is needed and, thus, the plume propagation is not influenced by the propulsion system,
- integral measurements over the path of the laser beam enable tomographic reconstruction of gas plumes and a localization of their source, and

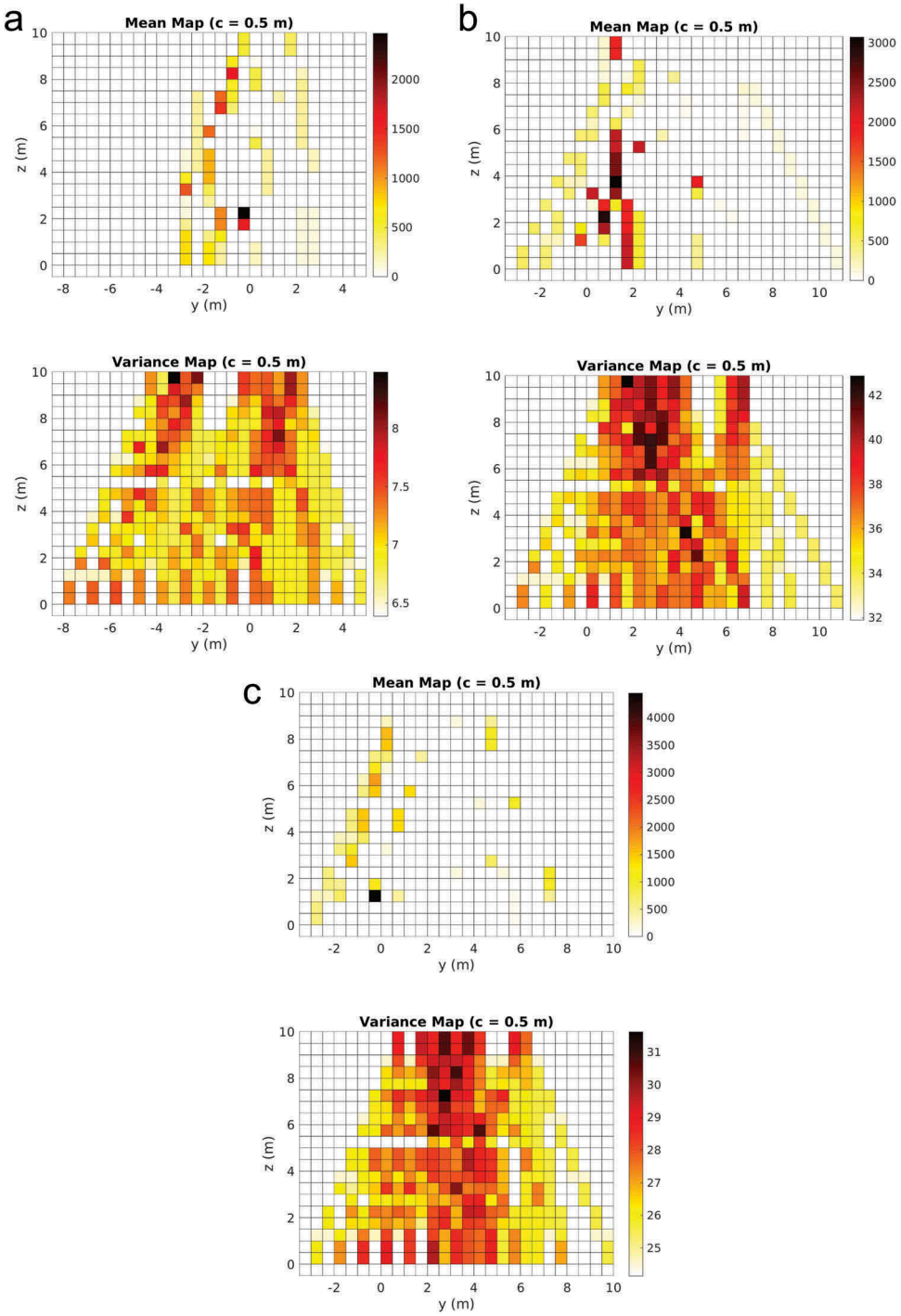

Figure 10. Reconstructed gas distribution (mean and variance maps) of the 2D plume using a cell size of 0.5 m. Note that the mean map concentration is given in ppm.

- potential reduction of exploration time due to remote sensing (Arain et al., 2015).

This means that the robot can operate much easier in real scenarios and is less constrained by a limited mobility than previous gas-sensitive mobile and aerial robots (Kowadlo & Russell, 2008; Neumann et al., 2016).

The contributions of this paper, which builds upon the work presented in (Neumann et al., 2017), are manifold: First, we tested our platform outdoors on the BAM TTS in three different scenarios to estimate the performance of the system. We used a CH_4 filled glass cube as a gas source and the results demonstrate that our platform can contribute to the task of monitoring, e.g. landfills and pipelines. Second, we extended a tomographic reconstruction algorithm first proposed in (Trincavelli et al., 2012) by a ray tracer to calculate the endpoint of the laser beam. Third, we built a unique experimental setup that allows for a quantitative or ground truth evaluation of algorithms in the field of aerial-based gas tomography. Fourth, we used this experimental setup to estimate the performance of the system in reconstructing 2D slices of a gas plume. To the best of our knowledge, this was the first time that a

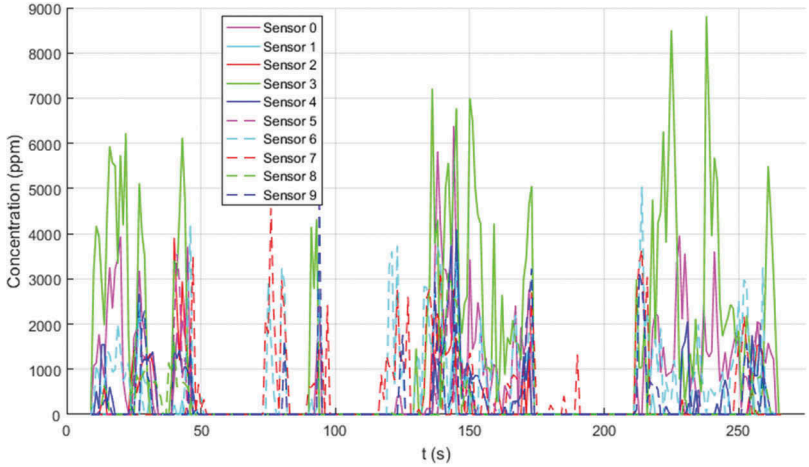

Figure 11. Methane concentration in ppm measured by the reference gas sensor array during trial #4 performed on day #1.

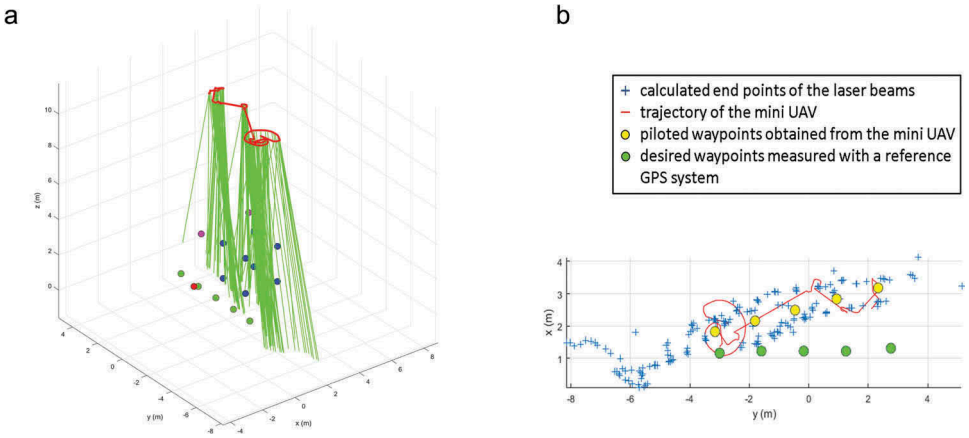

Figure 12. Experimental results of trial #4 performed on day #1: (a) 3D and (b) top view (2D) showing the calculated end points of the laser beams (blue points), the trajectory of the mini UAV (red line) and the piloted waypoints obtained from the mini UAV (yellow circles). The green circles mark the desired waypoints measured with a reference GPS system (Trimble Geo 7X, Trimble Inc., USA) that has centimeter accuracy. The location of the gas source, the anemometers and the aluminum metal frame cube is marked with red, purple and blue circles, respectively.

2D reconstruction of a gas plume was performed using an aerial robot equipped with a 3-axis gimbal mounted TDLAS sensor.

For future work, we plan to develop algorithms for the tomographic reconstruction of gas plumes and a precise localization of their sources, both in 3D. We will validate these algorithms by using the obtained measurement data set and by performing further field tests that will be supported by the distributed reference gas sensors that will be set up with a larger distance to each other. The main challenges of reconstructing gas plumes from integral measurements are the development of algorithms that cope with, i.e. the highly dynamic nature of gas dispersion (that is based on airflow advection and turbulence (Bennetts et al., 2014)), the sparsity of the measurements (the number of optical paths rarely exceeds 100 (Verkruysse & Todd, 2005)), the measurement geometry (measurement positions and orientations may affect the reconstruction quality (Hartl, Song, & Pundt, 2006)) and parameter selection (e.g. the cell size for grid-based approaches).

Furthermore, we plan to equip the mini UAV with an in-situ gas sensor for CH_4 (or even a sensor array to detect other compounds of interest, e.g. other combustible gases). This sensing payload can bring several advantages: For example, in case of a high concentration reading, the robot can decide whether it is located in a potentially explosive atmosphere or not and initiate an appropriate evasion strategy. While the TDLAS sensor provides remote measurements of the gas concentration, and thus enables to efficiently inspect large areas, the in-situ sensor could provide absolute concentration measurements close to a potential leak using calibrated chemical sensors (Bennetts et al., 2013). The in-situ sensor could be additionally used to verify the resolved integral concentration measurements. The miniaturization of the TDLAS sensor and thus the 3-axis gimbal is also an open issue we would like to address.

Future work will also aim at an improvement of the localization and attitude estimation of the mini UAV and its payload in outdoor environments (Neumann et al., 2017). Errors that occur here are particularly severe when a TDLAS sensor is used, as the resulting misalignments of the TDLAS beams have a big influence (Bennetts et al., 2013). To address this point, we plan, i.a., to equip the mini UAV with a D-RTK GNSS (Real Time Kinematic) high-precision navigation and positioning system that should allow centimeter-level positioning accuracy, both horizontally and vertically.

Acknowledgments

We would like to thank all participating colleagues and BAM for funding this interdisciplinary in-house R&D project. Furthermore, the authors would like to express their gratitude to the German Federal Ministry for Economic Affairs and Energy (BMWi) for funding a related project (grant number KF2201091HM4) within the ZIM program.

Disclosure statement

No potential conflict of interest was reported by the authors.

References

Arain, M.A., Schaffernicht, E., Hernandez Bennetts, V., & Lilienthal, A.J. (2016). The right direction to smell: Efficient sensor planning strategies for robot assisted gas tomography. In *Proceedings of the IEEE International Conference on Robotics and Automation (ICRA)*,Stockholm, Sweden, May 16-21, (pp. 4275–4281).

Arain, M.A., Trincavelli, M., Cirillo, M., Schaffernicht, E., & Lilienthal, A.J. (2015). Global coverage measurement planning strategies for mobile robots equipped with a remote gas sensor. *Sensors*, *15*(3), 6845–6871. doi:10.3390/s150306845

Bennetts, V.H., Lilienthal, A., Khaliq, A.A., Pomareda Sesé, V., & Trincavelli, M. (2012). Gasbot: A mobile robotic platform for methane leak detection and emission monitoring. In *IROS Workshop on Robotics for Environmental Monitoring (WREM)*, Vilamoura, Portugal, October 7-12

Bennetts, V.H., Lilienthal, A., Khaliq, A.A., Pomareda Sesé, V., & Trincavelli, M. (2013). Towards Real-World Gas Distribution Mapping and Leak Localization Using a Mobile Robot with 3D and Remote Gas Sensing Capabilities. In *Proceedings of the IEEE International Conference on Robotics and Automation (ICRA)*. Karlsruhe, Germany.

Bennetts, V.H., Schaffernicht, E., Stoyanov, T., Lilienthal, A.J., & Trincavelli, M. (2014). Online Robot Assisted Gas Tomography - Localizing Methane Leaks in Outdoor Environments. In *Proceedings of the IEEE International Conference on Robotics and Automation (ICRA)*. Hong Kong, China.

Bonow, G., & Kroll, A. (2013). Gas leak localization in industrial environments using a TDLAS-based remote gas sensor and autonomous mobile robot with the Tri-Max method. In *Proceedings of the IEEE International Conference on Robotics and Automation (ICRA)*. Karlsruhe, Germany.

Byer, R. (1979). Two-dimensional remote air-pollution monitoring via tomography. *Optics Letters*, *4*(3), 75–77.

DJI. (2016, January). *Spreading Wings S1000+, User Manual V1.4*. visited on 2016-07-01. Retrieved from http://dl.djicdn.com/downloads/s1000_plus/en/S1000+_User_Manual_en_v1.4.pdf

Drescher, A., Gadgil, A., Price, P., & Nazaroff, W. (1996). Novel approach for tomographic reconstruction of gas concentration distributions in air: Use of smooth basis functions and simulated annealing. *Atmospheric Environment*, *30*(6), 929–940. doi:10.1016/1352-2310(95)00295-2

Emran, B.J., Tannant, D.D., & Najjaran, H. (2017). Low-altitude aerial methane concentration mapping. *Remote Sensing*, *9*(8), 1-13.

Frish, M.B., Wainner, R.T., Green, B.D., Laderer, M.C., & Allen, M.G. (2005). Standoff gas leak detectors based on tunable diode laser absorption spectroscopy. In Alexey A. Belyanin, Rebekah A. Drezek, Claire F. Gmachl (Eds.), *Infrared to Terahertz Technologies for Health and the Environment, 6010* (pp. 1–9). SPIE Proceedings.

Frish, M.B., Wainner, R.T., Laderer, M.C., Allen, M.G., Rutherford, J., Wehnert, P., … Furry, D. (2013). Low-cost lightweight airborne laser-based sensors for pipeline leak detection and reporting. *Proc. SPIE, 8726*, 87260C-87260C-9.

Gaile, G.L., & Burt, J.E. (1980). *Directional Statistics. Concepts and Techniques in Modern Geography* (Vol. 25). Norwich, England: Institute of British Geographers.

Grinham, A., Dunbabin, M., Gale, D., & Udy, J. (2011). Quantification of ebullitive and diffusive methane release to atmosphere from a water storage. *Atmospheric Environment*, *45*(39), 7166–7173. doi:10.1016/j.atmosenv.2011.09.011

Hartl, A., Song, B., & Pundt, I. (2006). 2-d reconstruction of atmospheric concentration peaks from horizontal long path DOAS tomographic measurements: Parametrisation and geometry within a discrete approach. *Atmospheric Chemistry and Physics*, *6*(3), 847–861. doi:10.5194/acp-6-847-2006

Haruta, N., & Ogawa, K. (2005). Evaluation of Iterative Methods for Aperture Correction in SPECT. *Systems and Computers in Japan*, *36*(2), 52–61. doi:10.1002/scj.20158

Kowadlo, G., & Russell, R.A. (2008). Robot Odor Localization: A Taxonomy and Survey. *The International Journal of Robotics Research*, *27*(8), 869–894. doi:10.1177/0278364908095118

Lilienthal, A.J., Loutfi, A., & Duckett, T. (2006). Airborne Chemical Sensing with Mobile Robots. *Sensors*, *6*, 1616–1678. doi:10.3390/s6111616

Mahony, R., Hamel, T., & Pflimlin, J.-M. (2008). Nonlinear Complementary Filters on the Special Orthogonal Group. *IEEE Transactions on Automatic Control, Institute of Electrical and Electronics Engineers*, *53*(5), 1203–1217. doi:10.1109/TAC.2008.923738

Neumann, P.P., Asadi, S., Lilienthal, A.J., Bartholmai, M., & Schiller, J. (2012). Autonomous Gas-Sensitive Microdrone: Wind Vector Estimation and Gas Distribution Mapping. *IEEE Robotics and Automation Magazine*, *19*(1), 50–61. doi:10.1109/MRA.2012.2184671

Neumann, P.P., Bennetts, V.H., Lilienthal, A.J., & Bartholmai, M. (2016). From Insects to Micro Air Vehicles—A Comparison of Reactive Plume Tracking Strategies. In E. Menegatti, N. Michael, K. Berns, & H. Yamaguchi (Eds.), *Intelligent Autonomous Systems 13: Proceedings of the 13th*

international conference IAS-13 (pp. 1533–1548). Cham: Springer International Publishing.

Neumann, P.P., Bennetts, V.H., Lilienthal, A.J., Bartholmai, M., & Schiller, J.H. (2013). Gas source localization with a micro-drone using bio-inspired and particle filter-based algorithms. *Advanced Robotics*, *27*(9), 1–14. doi:10.1080/01691864.2013.779052

Neumann, P.P., Hüllmann, D., Krentel, D., Kluge, M., Kohlhoff, H., & Lilienthal, A.J. (2018). Gas Tomography Up in The Air! In *Proceedings of the IEEE Sensors conference*. Pullman New Delhi Aerocity, New-Delhi, India.

Neumann, P.P., Kohlhoff, H., Hüllmann, D., Lilienthal, A. J., & Kluge, M. (2017). Bringing Mobile Robot Olfaction to the Next Dimension – UAV-based Remote Sensing of Gas Clouds and Source Localization. In *Proceedings of the IEEE International Conference on Robotics and Automation (ICRA)*. ands Expo and Convention Centre, Marina Bay Sands, Singapore.

Price, P., Fischer, M., Gadgil, A., & Sextro, R. (2001). An algorithm for real-time tomography of gas concentrations, using prior information about spatial derivatives. *Atmospheric Environment*, *35*(16), 2827–2835. doi:10.1016/S1352-2310(01)00082-6

Ro, K.S., Johnson, M.H., Varma, R.M., Hashmonay, R.A., & Hunt, P. (2009). Measurement of greenhouse gas emissions from agricultural sites using open-path optical remote sensing method. *Journal of Environmental Science and Health, Part A*, *44*(10), 1011–1018. doi:10.1080/10934520902996963

Soldan, S., Bonow, G., & Kroll, A. (2012). 1st IFAC Workshop on Automatic Control in Offshore Oil and Gas Production RoboGasInspector - A Mobile Robotic System for Remote Leak Sensing and Localization in Large Industrial Environments: Overview and First Results. *IFAC Proceedings Volumes*, *45*(8), 33–38. doi:10.3182/20120531-2-NO-4020.00005

Tannant, D., Smith, K., Cahill, A., Hawthorne, I., Ford, O., Black, A., & Beckie, R. (2018). *Evaluation of a drone and laser - based methane sensor for detection of fugitive methane emissions (Tech. Rep.)*. Submitted to BC Oil and Gas Research and Innovation Society. University of British Columbia.

Tokyo Gas Engineering Co. Ltd (2013). *SA3C50A, LaserMethane mini-G, Operation Manual*. visited on 2016-07-01 Retrieved from https://www.crowcon.com/product/download/640/SA3C50A+Manual.pdf

Trincavelli, M., Bennetts, V.H., & Lilienthal, A. (2012). A Least Squares approach for learning gas distribution maps from a set of integral gas concentration measurements obtained with a TDLAS sensor. In *Proceedings of the IEEE Sensors conference*, Taipei International Convention Center, Taipei, Taiwan, (p. 1–4).

Verkruysse, W., & Todd, L.A. (2005). Novel algorithm for tomographic reconstruction of atmospheric chemicals with sparse sampling. *Environmental Science & Technology*, *39*(7), 2247–2254.

Yang, S., Talbot, R.W., Frish, M.B., Golston, L.M., Aubut, N.F., Zondlo, M.A., … McSpiritt, J. (2018). Natural gas fugitive leak detection using an unmanned aerial vehicle: Measurement system description and mass balance approach. *Atmosphere*, *9*(10). doi:10.3390/atmos9100383